Continuum Electrostatic Model for the Binding of Cytochrome c_2 to the Photosynthetic Reaction Center from *Rhodobacter sphaeroides*†

Osamu Miyashita, José N. Onuchic, and Melvin Y. Okamura*

Center for Theoretical Biological Physics and Department of Physics, University of California at San Diego, 9500 Gilman Drive, La Jolla, California 92093

Received June 16, 2003; Revised Manuscript Received August 12, 2003

ABSTRACT: Electrostatic interactions are important for protein−protein association. In this study, we examined the electrostatic interactions between two proteins, cytochrome c_2 (cyt c_2) and the reaction center (RC) from the photosynthetic bacterium *Rhodobacter sphaeroides*, that function in intermolecular electron transfer in photosynthesis. Electrostatic contributions to the binding energy for the cyt c_2−RC complex were calculated using continuum electrostatic methods based on the recent cocrystal structure [Axelrod, H. L., *et al*. (2002) *J. Mol. Biol*. *319*, 501−515]. Calculated changes in binding energy due to mutations of charged interface residues agreed with experimental results for a protein dielectric constant ϵ_{in} of 10. However, the electrostatic contribution to the binding energy for the complex was close to zero due to unfavorable desolvation energies that compensate for the favorable Coulomb attraction. The electrostatic energy calculated as a function of displacement of the cyt c_2 from the bound position showed a shallow minimum at a position near but displaced from the cocrystal configuration. These results show that although electrostatic steering is present, other short-range interactions must be present to contribute to the binding energy and to determine the structure of the complex. Calculations made to model the experimental data on association rates indicate a solvent-separated transition state for binding in which the cyt c_2 is displaced ∼8 Å above its position in the bound complex. These results are consistent with a two-step model for protein association: electrostatic docking of the cyt c_2 followed by desolvation to form short-range van der Waals contacts for rapid electron transfer.

Interprotein electron transfer plays an important role in the biological processes of photosynthesis and respiration (*1*−*3*). In these systems, water-soluble electron transport proteins, such as *c*-type cytochromes, shuttle between specific membrane-bound electron donor and acceptor proteins. Efficient electron transport in these systems requires a specific binding of the electron carrier so that the redox cofactors are close enough for the electron transfer reaction to proceed and fast enough so that rapid association and dissociation rates do not limit the electron flow. Electrostatic interactions play an important role in bringing the two proteins together for electron transfer. In this study, we examine electrostatic interactions between the reaction center (RC)[1] and cytochrome c_2 from the photosynthetic bacterium *Rhodobacter sphaeroides* using the recently determined X-ray crystal structure of the cyt c_2−RC complex (*4*) to determine their role in the association process.

Protein−protein association processes have been studied by several theoretical and experimental methods (for general reviews, see refs *2*, *3*, and *5*−*7*). The studies can typically be categorized as calculation of binding affinities (*8*−*16*), prediction of unknown bound structures (*17*−*24*), or modeling the kinetics of the binding process (*25*−*31*). Proteins can be characterized as fast binders ($k_{on} > 10^8$ M^{-1} s^{-1}) or slow binders ($k_{on} < 10^7$ M^{-1} s^{-1}) (*7*). The binding process of the fast binders is diffusion-limited and controlled by long-range "electrostatic steering" (*32*−*34*), and it exhibits a strong dependence on ionic concentration. One the other hand, the slow binders are controlled by shorter-range interactions and are less dependent on ion concentration. For the general mechanism of the binding process, a two-step mechanism has been discussed (*5*, *7*, *28*, *35*). The first step is diffusional association to form an encounter complex. Following the first step, the second step is rearrangement to form the fully bound complex. Short-range interactions such as van der Waals interactions are important at this stage.

The RC is the membrane protein involved in the initial light-induced electron transfer step in membranes of photosynthetic bacteria (for reviews see refs *36* and *37*). Light-induced electron transfer in RCs results in the oxidation of a primary donor, D, a bacteriochlorophyll dimer, and the reduction of a bound quinone Q. A water-soluble cyt c_2 transfers an electron to the RC, connecting the RC with the cytochrome bc_1 complex and completing the electron transfer cycle, resulting in proton pumping across the membrane and generation of a membrane potential driving ATP synthesis. The mechanism of the binding process and electron transfer reactions between cyt c_2 and the detergent-solubilized RCs

† This work was funded by the National Science Foundation-sponsored Center for Theoretical Biological Physics (Grants PHY-0216576 and 0225630), by National Science Foundation Grant MCB99-74568 to M.Y.O., and by a postdoctoral fellowship to O.M. from the La Jolla Interfaces in Science (LJIS), supported by the Burroughs Wellcome Fund.

* To whom correspondence should be addressed. Phone: (858) 534-2505. Fax: (858) 822-0007. E-mail: mokamura@ucsd.edu.

[1] Abbreviations: cyt c_2, cytochrome c_2; RC, reaction center.

10.1021/bi0350250 CCC: $25.00
Published on Web 09/20/2003

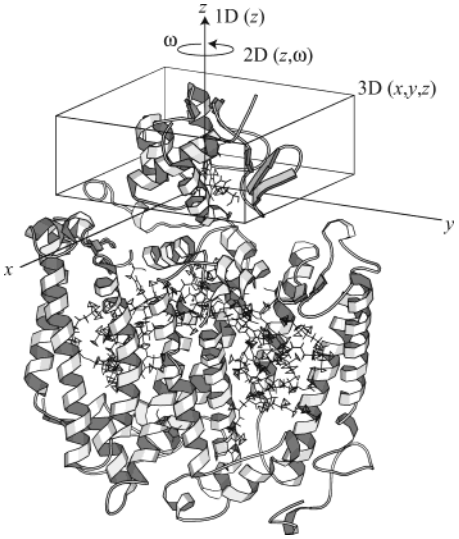

FIGURE 1: Representation of the cyt c_2−RC structure, showing the heme position above the BChl dimer. The coordinates varied in this study are shown. (1) One-dimensional translation, in which cyt c_2 is displaced from the reaction center (RC) surface along the perpendicular z direction. (2) Two-dimensional translation, rotation, in which cyt c_2 is displaced from the RC along the direction and rotated by an angle ω around the z axis. (3) Three-dimensional translation (no rotation), in which cyt c_2 is displaced in three dimensions (x, y, and z) in the space above the RC surface, but in which the orientation of cyt c_2 is fixed in the cocrystal orientation. The H subunit of RC is not included in our calculations.

have been extensively studied (*4*, *38*−*44*). The reaction scheme can be described as follows (*37*):

$$\begin{array}{ccc} \mathrm{cyt}^{2+} + \mathrm{DQ} & \xrightarrow{K_B = 1/K_D} & \mathrm{cyt}^{2+} : \mathrm{DQ} \\ h\nu \downarrow & & h\nu \downarrow \\ \mathrm{cyt}^{2+} + \mathrm{D}^{+}\mathrm{Q}^{-} & \underset{k_{off}}{\overset{k_{on}}{\rightleftharpoons}} & \mathrm{cyt}^{2+} : \mathrm{D}^{+}\mathrm{Q}^{-} \xrightarrow{k_e} \mathrm{cyt}^{3+} : \mathrm{DQ}^{-} \end{array}$$

When RCs are in the neutral state (DQ) and cyt c_2 equilibrates with a dissociation constant K_D in the dark, two populations of RCs are present, a fraction of RCs having bound cyt c_2 and a fraction with no bound cyt c_2. Following light excitation, the reaction shows at least two phases: a first-order phase ($k_e \sim 10^6$ s^{-1}), which corresponds to the electron transfer reaction rate of the already bound state, and a slower phase with a second-order rate constant k_2 (*37*), which is limited by the kinetics of docking of cyt c_2 to RC for those RCs lacking a bound cyt c_2. The second-order rate constant is dependent on ionic strength and is close to the diffusion limit at low ionic strengths ($k_2 \sim 10^9$ M^{-1} s^{-1}, 5 mM) (*42*). Thus, the cyt c_2 and RC can be considered a fast binding system. The observation of biphasic kinetics as well as the finding that the second-order rate constant is independent of driving force for electron transfer (*38*) indicate that k_e is faster than k_{off} and that k_2 ($\sim k_{on}$) is determined by the kinetics for association rather than by the rate of electron transfer.

The X-ray crystal structure of the complex between the cyt c_2 and RC shows the cyt c_2 docked with the heme edge contacting Tyr L162 directly above the bacteriochlorophyll dimer (see Figure 1). Hydrophobic interactions, intermolecular hydrogen bonds, and a cation−π interaction contribute short-range contacts to orient the two proteins in the bound state of the complex. The close contact between

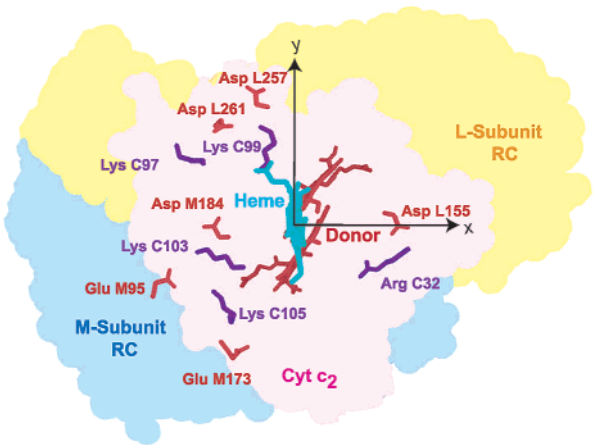

FIGURE 2: Top surface projection view of charged residues located in the interface region of the cyt c_2−RC complex showing acidic residues on the RC (red), basic residues on the cyt c_2 (purple), heme (magenta), and the BChl dimer donor (red). The RC L (yellow) and M (light blue) subunits and cyt c_2 (pink) are shown. The x and y axes are as indicated. The z axis is perpendicular to the plane of the page. The length of the arrow is 20 Å. Modified from Axelrod *et al.* (*4*).

the heme edge with the surface of the RC provides a strong tunneling pathway for electron transfer (*40*). Measurement of the rate of electron transfer from cyt c_2 to the RC in the crystal showed that the rate k_e (10^6 s^{-1}) was the same as that in solution, indicating that the configuration of cyt c_2 in the crystal is the same as the active configuration in solution. Charged residues on the cyt c_2 and RC are located in the binding interface between the two proteins. These are shown in projection from above the RC surface in Figure 2. A cluster of positively charged residues on cyt c_2 centered around Lys C103 are positioned opposite a cluster of negatively charged residues on the RC centered around Asp M184 in position for favorable electrostatic interaction. The oppositely charged residues are separated by distances of more than 4.5 Å, indicative of solvated charged residues.

The importance of electrostatic interactions for binding and association was shown by mutations of charged residues on the RC and cyt c_2 (*42*, *45*), by chemical modification studies (*46*), and by reactions with cytochromes from different species (*47*). Tetreault *et al.* (*42*) showed that mutation of charged residues on the RC resulted in changes in the second-order rate constant (k_2) and the dissociation constant (K_D). A log−log plot of k_2 versus $1/K_D$ (i.e., a free energy plot of rate vs binding) was linear with a slope α of $\sim$0.4. The slope (Brönsted coefficient), α, indicates a similarity between the structure of the transition state and that of the bound state. In this study, we analyze the electrostatic interaction between the cyt c_2 and RC in the bound complex (*4*) using a dielectric continuum model. Results from these calculations are compared to the experimental data. In addition, the electrostatic energy is examined as a function of the distance between the cyt c_2 and RC as the cyt c_2 is moved as a rigid body into its bound position in the complex. We show that electrostatic interactions are important for guiding the cyt c_2 and RC into proximity prior to binding but that electrostatic interactions alone do not determine the structure of the bound complex. In addition, a model for the transition state is proposed which explains the Brönsted coefficient ($\alpha = 0.4$).

METHODS

The binding free energy (ΔG) is defined as the difference in free energy between the bound and unbound states

$$\Delta G = G_{\text{bound}} - G_{\text{unbound}}$$

and it can be written in the form (*12*)

$$\Delta G = \Delta G_{\text{elec}} + \Delta G_{\text{np}} + \Delta G_{\text{strain}} - T\Delta S$$

where ΔG_{elec} and ΔG_{np} are the electrostatic and nonpolar contributions, respectively, to binding free energy. ΔG_{strain} accounts for possible distortions in the proteins upon complexation; however, this term would be small for the target system, since the structural change upon binding is found to be small (*4*). The last entropy term (ΔS) describes the loss of configurational entropy due to the loss of backbone and side chain torsional freedom, and translational and rotational degree of freedom upon complex formation.

While the nonpolar contributions are known to play an important role at the last stage of binding process, in this study we focus on the electrostatic contributions. The electrostatic contribution to the free energy for binding was calculated using a continuum electrostatic model. The protein molecules are treated as point charges within a region having a dielectric constant ϵ_{in} surrounded by solvent with a dielectric constant ϵ_{ext} of 80. The electrostatic free energy for binding is due to two types of interactions (*12*)

$$\Delta G_{\text{elec}} = \Delta G_{\text{coul}}(\epsilon_{\text{in}}) + \Delta G_{\text{solv}}(\epsilon_{\text{in}},\epsilon_{\text{ext}})$$

where $\Delta G_{\text{coul}}(\epsilon_{\text{in}})$ is the change in the pairwise Coulomb energy calculated between charges on different proteins using ϵ_{in} and $\Delta G_{\text{solv}}(\epsilon_{\text{in}},\epsilon_{\text{ext}})$ is the desolvation energy, the change in the electrostatic contribution to the solvation energy. The desolvation energy is due to the removal of high-dielectric water at the interface upon complex formation. In the continuum model, $G_{\text{solv}}(\epsilon_{\text{in}},\epsilon_{\text{ext}})$ is equal to the reaction field energy, the self-energy (Born energy) energy for transferring charges from a medium with a high dielectric constant ϵ_{ext} to a medium with a low dielectric constant ϵ_{in}, and ΔG_{solv} is the change in G_{solv} upon binding. The values for ΔG_{coul} and ΔG_{solv} are calculated from the X-ray crystal structures of the cyt c_2, RC, and cyt c_2−RC complex by solving the Poisson−Boltzmann equation using the program *DelPhi* (*48*) with charge parameters from the AMBER force field (*49*) and atom radii parameters from PARSE (*50*). The protein surface was defined by rolling a ball with a radius of 1.4 Å over the molecule (*50*). Mutated residues were modeled into the structure of the complex using SwissPdb Viewer (*51*). The best configuration was selected by considering nonbonded clashes and hydrogen bonds, assuming that the positions of the nonmutated residues were not changed. Hydrogen atoms were added using the AMBER software package (*52*). Since these modifications and hydrogen addition may add structural crushes, for each structure, 100 steps of minimization for relaxing added hydrogen atoms were performed, and in addition, three schemes of minimization were performed (see Results) to obtain structures that were used in the electrostatic calculations. Computations were carried out using two steps of focusing. For the first step, the spacing grid was set to 1 Å and the protein complex filled 40% of the box. For the second step, these values were 0.5 Å and 80%, respectively. For each step, 1000 iterations were performed to achieve convergence. The exterior dielectric constant (ϵ_{ext}) was set to 80 through the study, and the interior dielectric constant (ϵ_{in}) was varied from 1 to 20 to fit the experiment data (see Results). The ionic strength was set to 0, since the corresponding experiments were carried out at a low ionic strength (~5 mM). Test calculations showed that the ionic strength did not have a significant effect on the calculated energies.

To evaluate the electrostatic energy changes during the binding process, one-, two-, and three-dimensional energy surfaces were calculated as cyt c_2 was displaced from its position in the complex. The coordinate axes for the displacements were defined as shown in Figure 1. The iron atom of heme in the complex was defined as the origin $O(0,0,0)$. The z axis was defined as the perpendicular vector connecting the heme Fe with the vector between the two Mg atoms in the special pair, defined as the y direction. The magnesium of D_L is located on the $y > 0$ side. (1) The one-dimensional surface was obtained by displacing the cyt c_2 along the z axis. (2) The two-dimensional surface was obtained by displacing the cyt c_2 along the z axis and rotating it around the z axis by an angle ω. (3) The three-dimensional surface was obtained by displacing the cyt c_2 as a rigid body from its position in the cocrystal structure without rotation. After displacement of the cyt c_2, an additional 100 steps of minimization were performed to relax unphysical contacts between atoms, prior to the calculation of the electrostatic interaction.

RESULTS

Changes in Electrostatic Energy Due to Mutation of Charged Residues. The role of electrostatic interactions in the binding process was examined using a dielectric continuum model. This model was tested by calculating changes in the binding free energy ($\delta\Delta G_{\text{elec}}$) resulting from mutating charged residues on the RC and comparing these calculated changes to the experimental results of Tetreault *et al.* (*42*). The charged residues mutated in this study do not make van der Waals contact with cyt c_2 (*4*). In addition, these mutations were found experimentally to have only small effects on the first-order rate constant for electron transfer from cyt c_2 to RC. Thus, we assume that the orientations of the bound cyt c_2 in the mutant complexes are the same as that found in the native complex and that the changes in binding free energy are due to the change in electrostatic interactions.

Calculations were performed for the mutations changing the charge of surface residues on the RC. The modified RCs were DK(M184) (i.e., Asp M184 → Lys), DK(L261), DK(M88), EK(M95), DK(M292), DK(L257), DK(L155), EK(M100), EK(M111), DN(M184), EQ(M95), DN(M292), DN(L261), QE(L258), and DK(L155)/DK(L257). From the calculated electrostatic contributions to the binding energy, ΔG_{elec}, of each mutant, the changes due to mutations [i.e., $\delta\Delta G_{\text{elec}} = \Delta G_{\text{elec}}(\text{mutant}) - \Delta G_{\text{elec}}(\text{wild type})$] are obtained for different values of ϵ_{in}, and compared to experimental measurements (*42*). The results with an internal dielectric constant ϵ_{in} of 10 are shown in Figure 3. Quantitative agreement between the calculated and experimental values for the free energy was found (slope $a = 1.0$). Other values

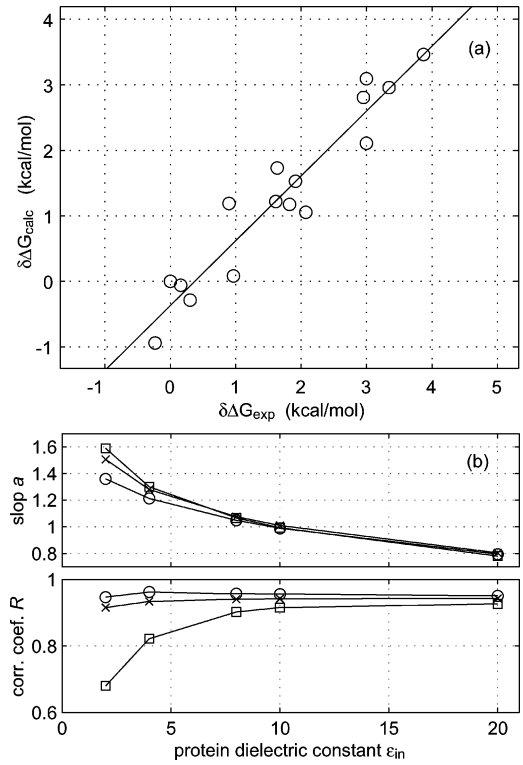

FIGURE 3: Calculated and experimental values for the change in binding free energy ($\delta\Delta G_{binding}$) due to mutation of charged residues on the RC. (a) Plot of the best fit between theory and experiment obtained using an ϵ_{in} of 10. The slope *a* equals 1.0. (b) Effect of internal dielectric constants (ϵ_{in}) and minimization scheme on the comparison of $\delta\Delta G_{binding}$ between calculation and experiments on the slope *a* and correlation coefficient *R*. Three minimization schemes, mutated residue only (×), 100 steps with all residues (○), and 1000 steps with all residues (□), are compared. Linear fitting of computational results to experimental results is performed for each mutation, which gives the relation $\delta\Delta G_{calc} = a\delta\Delta G_{exp} + b$. *R* is the correlation coefficient between experimental and computational data. Regardless of the minimization condition, an ϵ_{in} of 10 gives the quantitatively best agreement with the experimental value; i.e., the slope equals 1.00. The 100 steps minimization gives the best correlation.

of ϵ_{in} also show good correlation, i.e., correlation coefficient *R* of ~1. The experimental data could be fairly well fit by a range of ϵ_{in} values of 2−20 (slopes $a = 1.2-0.8$). These results support the model used in the calculation and indicate that the orientation of the cyt c_2 in the complex is not changed by the mutation.

The dielectric constant in the dielectric continuum model calculations implicitly includes electronic and nuclear relaxations responding to the change in charge distributions, and thus, the structure used for calculation may affect the optimal dielectric constant obtained in the above calculations (for example, see ref *53*). In particular, the scheme of minimization, which introduces relaxation in structure due to the mutations, would have an affect. Thus, we tested three minimization schemes: (1) 100 steps of minimization of only the mutated residue (other residues are fixed), (2) scheme 1 plus 100 steps of minimization of side chains of all residues (main chain atoms are fixed), and (3) 1000 steps of minimization allowing motion of all side chains. The results of these calculations are shown in Figure 3b. Calculations with scheme 2 showed smaller values of slope *a* than scheme 1. The best slope for both schemes 1 and 2 was obtained with an ϵ_{in} of 10. The best correlation coefficient was

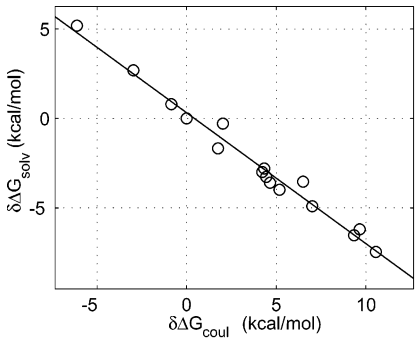

FIGURE 4: Calculated changes in the reaction field energy ($\delta\Delta G_{solv}$) and Coulomb energy ($\delta\Delta G_{coul}$) due to mutations of charged residues. The mutated residues were the same as in Figure 3. The plot shows that the two energies are linearly related; $\delta\Delta G_{solv} \sim -0.7\delta\Delta G_{coul}$.

obtained with scheme 2. Presumably, the relaxation allowed in scheme 2 is beneficial. However, the more extensive relaxation allowed by scheme 3 gives lower correlation coefficients, possibly due to distortions in structure introduced by long minimization without solvent. From these results, we selected Scheme 2 for minimization in the following calculations. We continue to examine the effect of varying the dielectric constant, since a range of protein dielectric constants give good agreement with experimental data.

Coulomb and Desolvation Energies. The Coulomb and desolvation energy contributions to the changes in electrostatic energy due to mutation were also examined. Tetreault *et al*. (*42*) compared the change in binding free energy due to mutating negatively charged residues to either positively charged residues or neutral residues, i.e., "charge-reversing" (from negative to positive) or "charge-neutralizing" (from negative to neutral) mutations. The ratio of change in free energy due to the of two mutations (γ) was calculated

$$\gamma = \frac{\delta\Delta G(-) \rightarrow (0)}{\delta\Delta G(-) \rightarrow (+)}$$

For all of four sets, γ was close to $^1/_2$. From this result, since $^1/_2$ is the value one can expect from Coulomb's law, the authors concluded that the desolvation energy is small for this system.

Here, we reexamine this result with our calculations. For each of the mutations, $\delta\Delta G_{solv}$ and $\delta\Delta G_{coul}$ were calculated. The results, shown in Figure 4, show that the desolvation energy $\delta\Delta G_{solv}$ is not small. Instead, the desolvation energy was found to be proportional to the change in the Coulomb contribution to the free energy ($\delta\Delta G_{solv} \sim -0.7\delta\Delta G_{coul}$). Thus, the change in total electrostatic energy was proportional to the change in Coulomb interaction energy; $\delta\Delta G_{elec} \sim 0.3\delta\Delta G_{coul}$. Since in the continuum model $\delta\Delta G_{coul}$ is calculated from Coulomb's law using a dielectric constant ϵ equal to ϵ_{in}, this observation implies that we can estimate the change in the electrostatic interaction due to mutation from Coulomb's law with a single dielectric constant of $\sim^{10}/_{0.3}$ (~30) and explains the resulting γ of $^1/_2$. The origin of this linear relationship and its general applicability to other systems require further study. We should also note that the simple Coulomb relationship applies only when calculating $\delta\Delta G_{elec}$ but does not apply when calculating ΔG_{elec}.

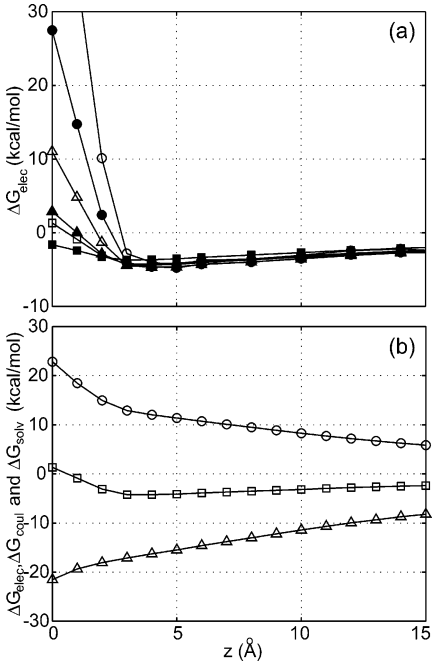

FIGURE 5: Electrostatic energy surface for one-dimensional translation along the *z* axis (a *z* of 0 corresponds to the cocrystal structure). (a) Total electrostatic energy vs distance for different dielectric constants. $\epsilon_{in} = 1$ (○), 2 (●), 4 (△), 8 (▲), 10 (□), and 20 (■). The minimum electrostatic energy is at ∼3 Å. At $z > 4$ Å, the electrostatic energy is almost independent of ϵ_{in}, since there is large solvent region (with $\epsilon_{ext} = 80$) between two molecules. At smaller values of *z*, the electrostatic energy becomes less favorable due to electrostatic desolvation. The desolvation effect is strongest for low values of ϵ_{in}. (b) Contributions to the total electrostatic energy calculated with an internal dielectric constant ϵ_{in} of 10: Coulomb interaction energy, ΔG_{coul} (△), reaction field (electrostatic solvation energy), ΔG_{solv} (○), and total electrostatic energy, ΔG_{elec} (□).

Electrostatic Energies at Different Docking Configurations. To elucidate the role of electrostatic energies in the docking and binding process, the electrostatic energies were calculated for different positions of the cyt c_2 relative the RC. Configurations of the cyt c_2 and RC were explored as the cyt c_2 moves away from the RC in one, two, and three dimensions. In these calculations, we assume that the cyt c_2 is oriented with the heme edge pointing toward the RC plane as in the crystal structure. This is reasonable since the cyt c_2 has a large dipole moment ($\mu = 120$ *e*Å) despite having only a small net charge of $-2e$. The front surface of the cyt c_2 containing the exposed heme edge is positively charged, and the binding surface of the RC has a strong negative charge. A preliminary study of the effects of rotation of the cyt c_2 perpendicular to the dipole axis was done by calculating the electrostatic energy of the system for rotation of the cyt c_2 around the *x* and *y* axes at $z = 10$ Å, $x = 0$, and $y = 0$. The value of ΔG_{elec}, calculated using the continuum model, was found to be close to a minimum when the cyt c_2 was in the cocrystal orientation. The average value of the rotation energy was increased by 1.6 kcal/mol for rotation of ±45° around the *x* and *y* axes, indicating that electrostatic interactions orient the cyt c_2 at the RC surface at this distance.

In the one-dimensional study, the electrostatic energy was calculated as a function of displacement of the cyt c_2 along the *z* direction, perpendicular to the RC surface using values of ϵ_{in} between 1 and 20 (Figure 5a). The total electrostatic energy is negative (favorable) as the cyt c_2 approaches the RC but goes through a minimum at a distance of ∼3 Å, independent of ϵ_{in}, and becomes less favorable at shorter distances. To understand the increase in energy at short distances, the two contributions to the electrostatic energy, the Coulomb interaction and the Poisson−Boltzmann reaction field energy, were calculated separately. The results for an ϵ_{in} of 10 are shown in Figure 5b. The Coulomb energy (ΔG_{coul}) decreased with decreasing distance, as expected for interactions between opposite charges. The reaction field energy (ΔG_{solv}) increased with decreasing distance, due to removal of the solvent from the charged interface. This increase in energy is attributed to the effect of desolvation; i.e., a closer approach would require the removal of solvent from charged residues. Similar results were found using different values of ϵ_{in} between 1 and 20. The repulsive effect of electrostatic desolvation is weaker for larger values of ϵ_{in}. It should be noted that in principle the best value for ϵ_{in} may be different at different values of *z*. However, the effect of varying ϵ_{in} is expected to be small and not significant at $z > 3$ Å. For all values of ϵ_{in}, the minimum electrostatic energy occurs at a distance longer than that observed in the crystal structure.

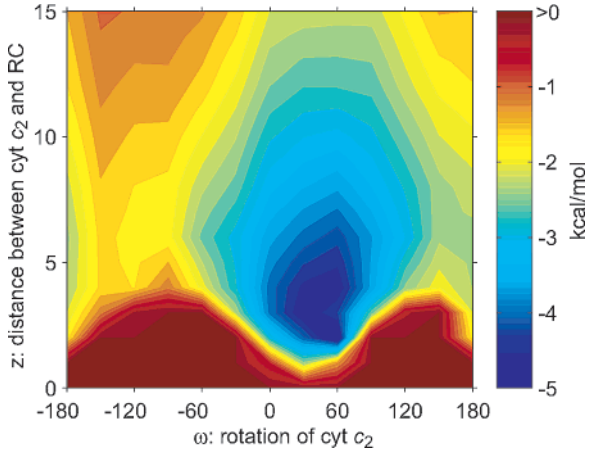

FIGURE 6: Two-dimensional electrostatic energy surface for *z* axis translation and rotation around the *z* axis. The minimum electrostatic energy configuration (dark blue) is close to that of the final state, but the cyt c_2 is displaced and rotated above the final position in the X-ray structure ($z = 3$ Å, $\omega \sim 40°$). Electrostatic interactions lead cyt c_2 toward the bound state (electrostatic steering); however, they do not determine the final structure of the complex (0,0).

In the two-dimensional study, the effect of rotating the cyt c_2 around the *z* axis at different values of *z* was examined. The two-dimensional energy surface calculated (using an $\epsilon_{in} = 10$) for translation and rotation is shown in Figure 6. A shallow minimum in the electrostatic energy was found at $z = 3$ Å and $\omega = 40°$. The position of this minimum was independent of ϵ_{in}. Thus, as the cyt c_2 approaches the RC surface, the electrostatic potential energy surface will tend to orient the cyt c_2 reasonably close to the orientation in the cocrystal structure. For *z* values of 5−10 Å, the energy difference between the favorable and unfavorable orientations is in the range of 1−2 kcal/mol (∼2−3k_BT), which is suitable for electrostatic steering. These results show that electrostatic interactions lead cyt c_2 near to the bound position; however, they do not determine the structure of the bound complex.

In the three-dimensional study, the effect of translating the cyt c_2 in a plane perpendicular to the *z* axis was examined. For simplicity, the cyt c_2 was translated along the *x*, *y*, and

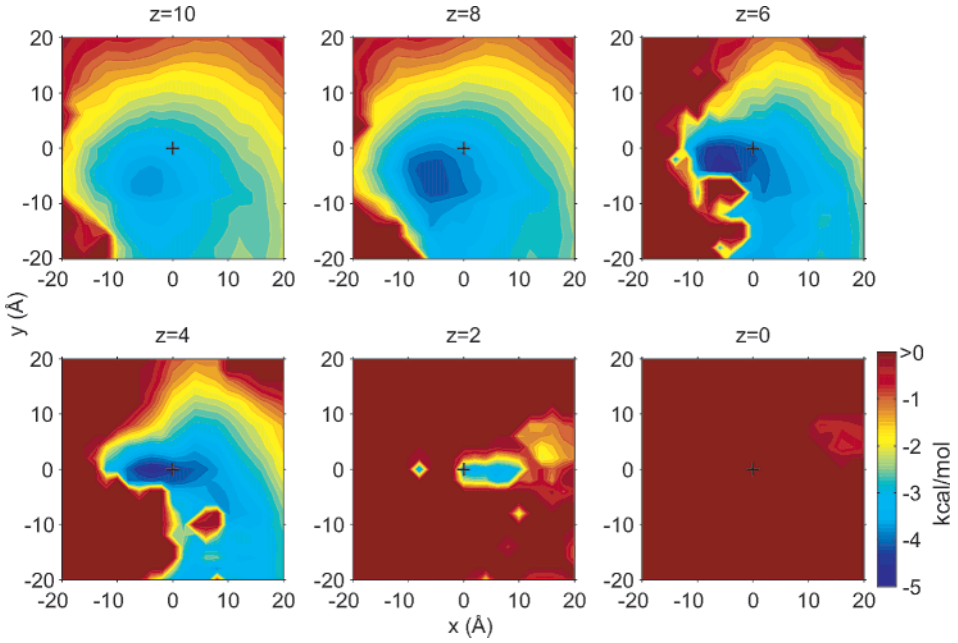

FIGURE 7: Three-dimensional electrostatic energy surfaces for translation of cyt c_2 with respect to the RC surface. The electrostatic energy in the $x-y$ plane is shown at different values of z. The cyt c_2 is fixed in the orientation of the cocrystal structure. The cross at the origin indicates the position of the bound complex. The electrostatic energy decreases as the cyt c_2 approaches the RC surface (electrostatic steering). The minimum electrostatic energy occurs when the cyt c_2 is displaced to a position ($x = -5$ Å, $y = 0$, and $z = 6$ Å) reasonably close to the position of the final complex. In this configuration, the heme is roughly located above Asp M184 (see Figure 2). Some of the unfavorable energy configurations (red regions at $z < 6$) are due to spatial overlap of the two protein surfaces.

z directions without rotation. The electrostatic energies in the $x-y$ plane for different values of z are shown in Figure 7. At $z = 10$ Å, a broad minimum is found near the position of the bound complex at the origin but displaced to x and y values of -5 and -5 Å, respectively. At smaller values of z, the position of the minimum shifts. At $z = 2$, the potential energy surface is greatly restricted to values near the bound configuration. This is partly due to the steric constraints due to fixing the cyt c_2 configuration to that of the bound state. This energetic restriction is indicative of a steering effect. However, as in the one- and two-dimensional studies, the position of minimum energy, near x and y values of approximately -5 and -3 Å, respectively, for $z \sim 6$ Å, does not correspond to the position of the bound complex.

Comparison between the Electrostatic Energy at Different Distances with Transition State Energies. In this section, calculations that model the transition state for the association process are presented. Experimentally, a Brönsted coefficient α of 0.4 was observed for mutations of charged residues on the RC (*42*). To characterize the structure of the transition state, we model it as a state in which the cyt c_2 is displaced linearly along the z direction without rotation from its orientation in the bound state. The change in electrostatic energy $\delta\Delta G(z)$ due to mutation of a residue was calculated with the cyt c_2 a distance z from its bound state. The ratio of the energy change $\delta\Delta G(z)/\delta\Delta G°(z=0)$ was taken to be the ratio of the change in transition state energy to the change in final state energy and should be equal to α. The best fit to an α of 0.40 from the calculations for the different mutations was obtained at a distance of 8 Å. This is shown in panels a and b of Figure 8. The optimal distance of 8 Å was independent of the dielectric constant from ϵ_{in} values of 1−10. Thus, these calculations are consistent with a transition state for binding in which cyt c_2 is located at $z \sim$ 8 Å above the RC compared to the X-ray cocrystal structure.

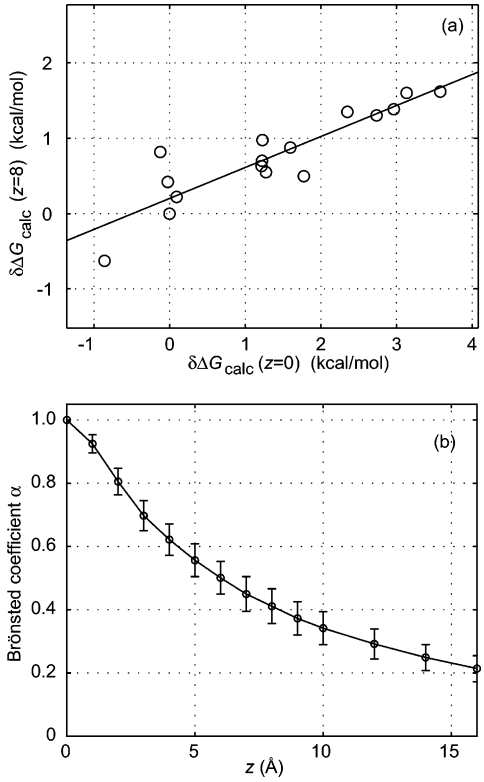

FIGURE 8: (a) Calculations modeling the Brönsted coefficient. The free energy changes for mutations in complexes displaced along z by 8 Å and 0 give a slope α of 0.41 ± 0.05, in agreement with the experimental value of 0.40. (b) Values of α for different displacements along the z axis. The best fit to an α of 0.40 is at a distance of 8 Å. This distance was almost independent of ϵ_{in}.

This would position the transition state near the region of minimum electrostatic energy (where x, y, and $z \sim -5$, -3, and 6 Å, respectively) discussed in the previous section.

Effect of Nonelectrostatic Contributions to the Binding Energy. In the simple model used in these calculations, it is assumed that the changes in binding energy due to mutation of charged residues are only due to electrostatic interactions. However, nonelectrostatic contributions (e.g., due to van der Waals contacts) may also be present. These contributions are not expected to be large since in the cyt c_2−RC complex the charged residues are not in van der Waals contact (*4*). In addition, the close fit of the binding energy by the electrostatic calculation suggests that electrostatic interactions dominate. The possible nonelectrostatic effects of mutation are expected to decrease the binding affinity due to unfavorable contacts. If a nonelectrostatic, positive contribution of 20% to the binding energy is assumed to be present, the parameters from the electrostatic calculations would be modified. The new parameters would be an optimal ϵ_{in} of ∼20 (Figure 3), a small favorable electrostatic contribution to the binding energy ΔG_{elec} of approximately −2 kcal/mol (Figure 5), and a lower limit for the distance z in the transition state of ∼6 Å (Figure 8, assuming that the transition state energy is totally electrostatic).

DISCUSSION

Electrostatic Contribution to the Binding Energy. In this study, the electrostatic energies between cyt c_2 and RC were calculated for the cyt c_2 positioned in the bound state or in configurations approaching the bound state. The continuum electrostatic model gave good agreement with experimental results for the free energy changes upon modification of charged surface residues on the RC when a protein dielectric constant of 10 was used (Figure 3). However, calculation of the electrostatic energy as a function of distance indicates that the electrostatic interaction does not dominate the binding energy but instead is close to zero and slightly unfavorable ($\Delta G_{elec} \sim 1$ kcal/mol at an ϵ_{in} of 10) when the cyt c_2 is in the position of the bound state (Figure 5). This indicates that other interactions, such as hydrophobic contacts, van der Waals interactions, and the entropy contribution of displaced water, must be considered to account for the binding energy.

The difference between the two results, i.e., the changes in free energy upon mutation and the relatively unchanged total energy, are not contradictory since the total electrostatic energy for binding (ΔG_{elec}) is not equal to the sum of the changes in free energy $\delta\Delta G_{elec}$ due to mutation of single residues as pointed out by Hendsch and Tidor (*54*). This occurs because the contribution of each residue to the total binding energy is the desolvation energy plus one-half of the Coulomb energy due to the residue. However, the replacement of a residue with a different residue by mutation results in a change in the desolvation energy and the loss of all of the Coulomb energy due to the residue (for the case of mutation to a neutral residue). Thus, mutational results tend to overemphasize the Coulomb contribution compared to the desolvation effects.

The small unfavorable electrostatic contribution to the binding energy is somewhat surprising in view of the large number of complementary charged residues on cyt c_2 and the RC in the interaction region. However, the unfavorable effects of desolvation leading to unfavorable free energies for burying charges due to protein association have been observed in other protein associations studied using Poisson−Boltzmann electrostatic calculations (*12*, *25*, *26*, *55*). This has been explained by the loss of the stabilization effect due to polarization of bulk water molecules (*56*, *57*). The exclusion of solvent generally destabilizes charges buried by the protein association process. The fact that in the cyt c_2−RC complex, the charges are not completely buried and in all cases are partially solvated (*4*) indicates that the system is designed to maximize the electrostatic contribution to the stability of the cyt c_2−RC complex by minimizing the electrostatic desolvation penalty. The partial solvation of the charged groups may also explain the relatively high ϵ_{in} value of 10 found to be optimal in this study (*16*).

Electrostatic Contribution to the Docking Process. Even though the electrostatic interactions do not enhance the binding energy, they play a key role in the docking process. A general feature of the docking calculations for different configurations is a minimum electrostatic energy when the cyt c_2 is close to the surface of the RC (Figures 5−7). The electrostatic energy surfaces show smooth decreases in energy that lead to an encounter complex in which the cyt c_2 is positioned within 5−10 Å of its position in the final complex. The relatively broad shallow energy profile allows the cyt c_2 to readily explore configurations near this minimum and to access the transition state leading to the final state active in electron transfer. This result agrees with the electrostatic analysis of Tiede *et al*. (*58*), who commented on the diffuse nature of the electrostatic potential energy surface of the cyt and RC, allowing cytochromes from a variety of different species to bind to the RC.

The absolute minimum for the electrostatic energy in the three-dimensional study was found at x and y values of approximately −5 and −3 Å, respectively, for a z of 6 Å (Figure 7). This would position the heme edge of the cyt c_2 above Asp M184 (see Figure 2). This position agrees with the placement of cyt c_2 based on electrostatic calculations reported by Adir *et al*. (*59*). However, it disagrees with the position of the cyt c_2 in the bound complex (*4*), showing that electrostatic interactions do not determine the structure of the bound state. This general feature of the energy surface was obtained with a simplified model in which the orientations of the cyt c_2 were in a restricted range. Although extensive evaluation of the energy surface over more configurations should lead to a more detailed energy profile, the general result of these calculations is expected to remain unchanged. In view of the relatively nonspecific nature of electrostatic interactions, short-range interactions must be invoked to account for the specific structure of the cyt c_2−RC complex observed in the crystal structure with cyt c_2 optimally positioned on the RC surface for electron transfer (*4*, *37*). Several possible short-range hydrophobic contacts between the heme edge and Phe C102 on the RC and Tyr L162 and Leu M191 on the RC and a cation−π contact between Arg C32 and Tyr M295 are observed in the crystal structure that may account for the specific binding (*4*). Thus, a "two-step mechanism" (*7*, *28*, *35*) can be applied to binding in this system. The binding process consists of the shift from an electrostatic interaction to van der Waals interactions.

Model for the Transition State. Electrostatic calculations were used to model the transition state for the association process. The method used in this study is an alternative to calculating the free energy as a function of position to obtain

the transition state and is based on fitting changes in rate due to mutation assuming that this change is due to electrostatic interactions. Experimental results from a Brönsted plot (*42*) and a double mutant study (*41*) showed that in the transition state the cyt c_2 was in an orientation similar to that of the final state. Using results from electrostatic calculations, we propose a model of the transition state that is consistent with experimental data. We make the simplifying assumption that our one-dimensional model, i.e., docking of the cyt c_2 along the z direction, is a representation of the association process. For this simple model, the best fit with a Brönsted coefficient α of 0.4 occurs at a z distance of 8 Å (Figure 8). Thus, the experimental results are best reproduced by a transition state in which the cyt c_2 is displaced by ~8 Å along the z axis away from the RC. In the proposed transition state, the van der Waals contacts between cyt c_2 and RC have not yet been formed and thus the transition state energy should be dominated by long-range electrostatic interactions while short-range interactions between uncharged residues should not be very important. This agrees with the observation that mutations to uncharged residues on the RC, Leu M192 and Tyr M295 involved in short-range hydrophobic and cation$-\pi$ interactions, respectively, have little effect on the second-order rate constant (i.e., Brönsted coefficient of ~0.1; X. M. Gong and K. Weber, unpublished results).

To a first approximation, the transition state corresponds to the peak in the free energy along the reaction coordinate (*60*). Since only the electrostatic contributions were represented in the plot shown in Figure 5a, no peak is present at $z = 8$ Å. This is expected since the free energy barrier results from enthalpic and entropic contributions that were not explicitly considered in our calculations. One possible contribution to the free energy barrier is the energy required for bond breaking when removing solvent water molecules between the two proteins. At $z = 8$ Å, there is enough separation that two or more solvent water layers are between the cyt c_2 and RC. This solvation layer impedes short-range interactions at the interface between the electron transfer cofactors, heme and $BChl_2$, where the surfaces come into van der Waals contact in the bound state. The energy for removal of the final layers of water bound to the two surfaces prior to formation of the complex may be responsible for the barrier (*26*, *61*). Another contribution to the free energy barrier for association is the loss of translational and rotational entropy due to association. Zhou has demonstrated that a peak in a smooth electrostatic potential surface, such as Figure 5a, may be produced by including the change in the translational entropy with distance (*62*).

The proposed model for the transition state is consistent with the transition state descriptions for other fast binding systems (*4*, *5*, *28*, *29*). Seltzer and Schreiber have analyzed the transition state for the association of barnase and barstar using an electrostatic calculation similar that that used in the study presented here (*63*). They calculated the effect of mutations to the energy of an encounter complex having space for one water molecule between the two proteins and obtained a Brönsted coefficient of 0.8 for a log plot of the association rate versus the electrostatic energy calculated for the encounter complex. This result could be explained if the transition state was positioned at a larger distance than that of the encounter complex, separated by the diameter of two or more water molecules, consistent with our study. Frisch *et al*. have analyzed the association process of barnase and barstar (*29*). They find that interactions of charged residues are important for the transition states, while interactions of uncharged residues are not important. In addition, they concluded that the desolvation of the interface has not yet occurred from the observation that the activation entropy was close to zero.

We can characterize the electron transfer process more quantitatively by estimating the electron transfer rate as a function of distance of the cyt c_2 from the RC surface by using the exponential dependence of the rate of electron transfer with a distance k which equals $k_e e^{-\beta r}$ where $\beta = 1.61-1.75$ Å^{-1} for transfer through an aqueous interface (*64*). An electron transfer rate at the transition state (k_e) ~1 s^{-1} is obtained, a factor of 10^6 slower than in the bound state. A similar slow rate would be calculated for the cyt c_2 positioned at the electrostatic energy minimum. However, fluctuations in distance, bringing the cyt c_2 in closer contact with the active site, greatly increase the rate of electron transfer. The simplest model for the second-order electron transfer rate process is that the two proteins associate to form a cyt c_2-RC complex having the same structure as that of the cocrystal, in which the heme edge is in van der Waals contact with Tyr L162 on the RC. While this assumption is reasonable, we cannot rule out the possibility that electron transfer occurs at other configurations prior to formation of the thermodynamically stable state. The actual situation will depend on the rates of the binding to the active configuration compared to binding to inactive configurations and relative to the rates of electron transfer from different configurations (*65*). Although clear funnel-like behavior (electrostatic steering) was confirmed in the studies of the electrostatic landscape, the real binding process is likely to include a number of different paths. Thus, it is likely that the transition state is not a single structure but an ensemble of structures. However, since electrostatic interactions are long-range effects, the overall features of the transition state are expected to agree with the model presented here.

CONCLUDING REMARKS

In this study, we used a simple continuum model to calculate the electrostatic contribution to the energy surface for the binding between cytochrome c_2 (cyt c_2) and the bacterial reaction center (RC) from *R. sphaeroides*. The model was able to simulate experimental data on the effects of mutation of charged residues on binding and rates of association. These calculations indicate that electrostatic interactions play an important role in the rate of docking but are less important in determining the structure of the complex and do not make a major contribution to the binding energy. In addition, the transition state for association was characterized as a solvent-separated complex with the cyt positioned ~8 Å, the diameters of at least two water molecules, farther from the RC than in the bound state.

Further calculations are necessary to improve upon this simple electrostatic model and characterize the final step in binding. Steered molecular dynamics simulations provide a tool for this more detailed analysis by allowing for residue flexibility and explicit solvation. Preliminary results by

Luthey-Schulten and collaborators with this new approach are encouraging and will allow for more quantitative studies in the future (F. Autenrieth, K. Schulten, and Z. Luthey-Schulten, unpublished results). Detailed studies of the transition state should include the role of other configurations in the binding process and the role of electron transfer from different configurations. The theoretical and experimental mechanism, which may be used to explore this transition state ensemble in this problem, is similar to Φ value analysis in protein folding (*66*, *67*). Utilizing this approach, one will be able to identify the participation of individual amino acids at this transition state ensemble. Further studies of the binding energy should deal with the entropy of binding and calculation of the van der Waals interactions.

ACKNOWLEDGMENT

We thank Herb Axelrod, Mark Paddock, and George Feher for helpful discussions. Computations have been done at the University of California at San Diego Keck II computing facility (partially supported by National Science Foundation Grant 9970199) and the San Diego Supercomputer Center.

SUPPORTING INFORMATION AVAILABLE

Results of electrostatic calculations for an internal dielectric constant of 10 and one-dimensional study. This material is available free of charge via the Internet at http://pubs.acs.org.

REFERENCES

1. Cramer, W. A., and Knaff, D. B. (1990) in *Energy transduction in biological membranes: A textbook of bioenergetics*, Springer-Verlag, New York.
2. Bendall, D. S. (1996) in *Protein electron transfer* (Bendall, D. S., Ed.) pp 43−68, Bios Scientific, Oxford, U.K.
3. Mathews, F. S., Mauk, A. G., and Moore, G. R. (2000) in *Protein−protein recognition* (Kleanthous, C., Ed.) pp 60−101, Oxford University Press, New York.
4. Axelrod, H. L., Abresch, E. C., Okamura, M. Y., Yeh, A. P., Rees, D. C., and Feher, G. (2002) X-ray structure determination of the cytochrome c_2: Reaction center electron-transfer complex from *Rhodobacter sphaeroides*, *J. Mol. Biol. 319*, 501−515.
5. Schreiber, G. (2002) Kinetic studies of protein−protein interactions, *Curr. Opin. Struct. Biol. 12*, 41−47.
6. Elcock, A. H., Sept, D., and McCammon, J. A. (2001) Computer simulation of protein−protein interactions, *J. Phys. Chem. B 105*, 1504−1518.
7. Camacho, C. J., and Vajda, S. (2002) Protein−protein association kinetics and protein docking, *Curr. Opin. Struct. Biol. 12*, 36−40.
8. Kollman, P. A., Massova, I., Reyes, C., Kuhn, B., Huo, S. H., Chong, L., Lee, M., Lee, T., Duan, Y., Wang, W., Donini, O., Cieplak, P., Srinivasan, J., Case, D. A., and Cheatham, T. E. (2000) Calculating structures and free energies of complex molecules: Combining molecular mechanics and continuum models, *Acc. Chem. Res. 33*, 889−897.
9. Massova, I., and Kollman, P. A. (1999) Computational alanine scanning to probe protein−protein interactions: A novel approach to evaluate binding free energies, *J. Am. Chem. Soc. 121*, 8133−8143.
10. Noskov, S. Y., and Lim, C. (2001) Free energy decomposition of protein−protein interactions, *Biophys. J. 81*, 737−750.
11. Sheinerman, F. B., Norel, R., and Honig, B. (2000) Electrostatic aspects of protein−protein interactions, *Curr. Opin. Struct. Biol. 10*, 153−159.
12. Froloff, N., Windemuth, A., and Honig, B. (1997) On the calculation of binding free energies using continuum methods: Application to MHC class I protein-peptide interactions, *Protein Sci. 6*, 1293−1301.
13. Simonson, T., Archontis, G., and Karplus, M. (2002) Free energy simulations come of age: Protein−ligand recognition, *Acc. Chem. Res. 35*, 430−437.
14. Lamb, M. L., and Jorgensen, W. L. (1997) Computational approaches to molecular recognition, *Curr. Opin. Chem. Biol. 1*, 449−457.
15. Aqvist, J., Luzhkov, V. B., and Brandsdal, B. O. (2002) Ligand binding affinities from MD simulations, *Acc. Chem. Res. 35*, 358−365.
16. Muegge, I., Schweins, T., and Warshel, A. (1998) Electrostatic contributions to protein−protein binding affinities: Application to Rap/Raf interaction, *Proteins: Struct., Funct., Genet. 30*, 407−423.
17. DeLano, W. (2002) Unraveling hot spots in binding interfaces: Progress and challenges, *Curr. Opin. Struct. Biol. 12*, 14−20.
18. Smith, G., and Sternberg, M. (2002) Prediction of protein−protein interactions by docking methods, *Curr. Opin. Struct. Biol. 12*, 28−35.
19. Dennis, S., Kortvelyesi, T., and Vajda, S. (2002) Computational mapping identifies the binding sites of organic solvents on proteins, *Proc. Natl. Acad. Sci. U.S.A. 99*, 4290−4295.
20. Camacho, C. J., Gatchell, D. W., Kimura, S. R., and Vajda, S. (2000) Scoring docked conformations generated by rigid-body protein−protein docking, *Proteins: Struct., Funct., Genet. 40*, 525−537.
21. Verkhivker, G. M., Bouzida, D., Gehlhaar, D. K., Rejto, P. A., Freer, S. T., and Rose, P. W. (2002) Monte Carlo simulations of the peptide recognition at the consensus binding site of the constant fragment of human immunoglobulin G: The energy landscape analysis of a hot spot at the intermolecular interface, *Proteins: Struct., Funct., Genet. 48*, 539−557.
22. Mandell, J. G., Roberts, V. A., Pique, M. E., Kotlovyi, V., Mitchell, J. C., Nelson, E., Tsigelny, I., and Ten Eyck, L. F. (2001) Protein docking using continuum electrostatics and geometric fit, *Protein Eng. 14*, 105−113.
23. Verkhivker, G. M., Bouzida, D., Gehlhaar, D. K., Rejto, P. A., Freer, S. T., and Rose, P. W. (2002) Complexity and simplicity of ligand-macromolecule interactions: The energy landscape perspective, *Curr. Opin. Struct. Biol. 12*, 197−203.
24. Roberts, V. A., and Pique, M. E. (1999) Definition of the interaction domain for cytochrome *c* on cytochrome *c* oxidase. III. Prediction of the docked complex by a complete, systematic search, *J. Biol. Chem. 274*, 38051−38060.
25. Elcock, A. H., Gabdoulline, R. R., Wade, R. C., and McCammon, J. A. (1999) Computer simulation of protein−protein association kinetics: Acetylcholinesterase-fasciculin, *J. Mol. Biol. 291*, 149−162.
26. Camacho, C. J., Weng, Z. P., Vajda, S., and DeLisi, C. (1999) Free energy landscapes of encounter complexes in protein−protein association, *Biophys. J. 76*, 1166−1178.
27. Selzer, T., Albeck, S., and Schreiber, G. (2000) Rational design of faster associating and tighter binding protein complexes, *Nat. Struct. Biol. 7*, 537−541.
28. Selzer, T., and Schreiber, G. (2001) New insights into the mechanism of protein−protein association, *Proteins: Struct., Funct., Genet. 45*, 190−198.
29. Frisch, C., Fersht, A. R., and Schreiber, G. (2001) Experimental assignment of the structure of the transition state for the association of barnase and barstar, *J. Mol. Biol. 308*, 69−77.
30. De Rienzo, F., Gabdoulline, R. R., Menziani, M. C., De Benedetti, P. G., and Wade, R. C. (2001) Electrostatic analysis and Brownian dynamics simulation of the association of plastocyanin and cytochrome f, *Biophys. J. 81*, 3090−3104.
31. Gabdoulline, R. R., and Wade, R. C. (2002) Biomolecular diffusional association, *Curr. Opin. Struct. Biol. 12*, 204−213.
32. Sines, J. J., Allison, S. A., and McCammon, J. A. (1990) Point-charge distributions and electrostatic steering in enzyme substrate encounter: Brownian dynamics of modified copper−zinc superoxide dismutases, *Biochemistry 29*, 9403−9412.
33. Luty, B. A., Wade, R. C., Madura, J. D., Davis, M. E., Briggs, J. M., and McCammon, J. A. (1993) Brownian dynamics simulations of diffusional encounters between triose phosphate isomerase and glyceraldehyde phosphate: electrostatic steering of glyceraldehyde phosphate, *J. Phys. Chem. 97*, 233−237.
34. Gabdoulline, R. R., and Wade, R. C. (2001) Protein−protein association: Investigation of factors influencing association rates by Brownian dynamics simulations, *J. Mol. Biol. 306*, 1139−1155.

35. Camacho, C. J., and Vajda, S. (2001) Protein docking along smooth association pathways, *Proc. Natl. Acad. Sci. U.S.A. 98*, 10636−10641.
36. Feher, G., Allen, J. P., Okamura, M. Y., and Rees, D. C. (1989) Structure and function of bacterial photosynthetic reaction centers, *Nature 339*, 111−116.
37. Tiede, D. M., and Dutton, P. L. (1993) in *The photosynthetic reaction center* (Deisenhofer, J., and Norris, J. R., Eds.) pp 257−298, Academic Press, San Diego.
38. Lin, X., Williams, J. C., Allen, J. P., and Mathis, P. (1994) Relationship between rate and free energy difference for electron transfer from cytochrome c_2 to the reaction center in *Rhodobacter sphaeroides*, *Biochemistry 33*, 13517−13523.
39. Venturoli, G., Drepper, F., Williams, J. C., Allen, J. P., Lin, X., and Mathis, P. (1998) Effects of temperature and $\Delta G°$ on electron transfer from cytochrome c_2 to the photosynthetic reaction center of the purple bacterium *Rhodobacter sphaeroides*, *Biophys. J. 74*, 3226−3240.
40. Aquino, A. J. A., Beroza, P., Beratan, D. N., and Onuchic, J. N. (1995) Docking and electron transfer between cytochrome c_2 and the photosynthetic reaction center, *Chem. Phys. 197*, 277−288.
41. Tetreault, M., Cusanovich, M., Meyer, T., Axelrod, H., and Okamura, M. Y. (2002) Double mutant studies identify electrostatic interactions that are important for docking cytochrome c_2 onto the bacterial reaction center, *Biochemistry 41*, 5807−5815.
42. Tetreault, M., Rongey, S. H., Feher, G., and Okamura, M. Y. (2001) Interaction between cytochrome c_2 and the photosynthetic reaction center from *Rhodobacter sphaeroides*: Effects of charge-modifying mutations on binding and electron transfer, *Biochemistry 40*, 8452−8462.
43. Farchaus, J. W., Wachtveitl, J., Mathis, P., and Oesterhelt, D. (1993) Tyrosine 162 of the photosynthetic reaction center L-subunit plays a critical role in the cytochrome c_2 mediated rereduction of the photooxidized bacteriochlorophyll dimer in *Rhodobacter sphaeroides*. 1. Site-directed mutagenesis and initial characterization, *Biochemistry 32*, 10885−10893.
44. Wachtveitl, J., Farchaus, J. W., Mathis, P., and Oesterhelt, D. (1993) Tyrosine 162 of the photosynthetic reaction center L-subunit plays a critical role in the cytochrome c_2 mediated rereduction of the photooxidized bacteriochlorophyll dimer in *Rhodobacter sphaeroides*. 2. Quantitative kinetic analysis, *Biochemistry 32*, 10894−10904.
45. Caffrey, M. S., Bartsch, R. G., and Cusanovich, M. A. (1992) Study of the cytochrome c_2 reaction center interaction by site-directed mutagenesis, *J. Biol. Chem. 267*, 6317−6321.
46. Long, J. E., Durham, B., Okamura, M., and Millett, F. (1989) Role of specific lysine residues in binding cytochrome c_2 to the *Rhodobacter sphaeroides* reaction center in optimal orientation for rapid electron transfer, *Biochemistry 28*, 6970−6974.
47. Tiede, D. M., and Chang, C. H. (1988) The cytochrome *c* binding surface of reaction centers from *Rhodobacter sphaeroides*, *Isr. J. Chem. 28*, 183−191.
48. Honig, B., and Nicholls, A. (1995) Classical electrostatics in biology and chemistry, *Science 268*, 1144−1149.
49. Cornell, W. D., Cieplak, P., Bayly, C. I., Gould, I. R., Merz, K. M., Ferguson, D. M., Spellmeyer, D. C., Fox, T., Caldwell, J. W., and Kollman, P. A. (1995) A second generation force field for the simulation of proteins, nucleic acids, and organic molecules, *J. Am. Chem. Soc. 117*, 5179−5197.
50. Sitkoff, D., Sharp, K. A., and Honig, B. (1994) Accurate calculation of hydration free energies using macroscopic solvent models, *J. Phys. Chem. 98*, 1978−1988.
51. Guex, N., and Peitsch, M. C. (1997) SWISS-MODEL and the Swiss-PdbViewer: An environment for comparative protein modeling, *Electrophoresis 18*, 2714−2723.
52. Case, D. A., Pearlman, D. A., Caldwell, J. W., Cheatham, T. E., III, Ross, W. S., Simmerling, C. L., Darden, T. A., Merz, K. M., Stanton, R. V., Cheng, A. L., Vincent, J. J., Crowley, M., Tsui, V., Radmer, R. J., Duan, Y., Pitera, J., Massova, I., Seibel, G. L., Singh, U. C., Weiner, P. K., and Kollman, P. A. (1999) *AMBER*, University of California, San Francisco.
53. Simonson, T. (2001) Macromolecular electrostatics: Continuum models and their growing pains, *Curr. Opin. Struct. Biol. 11*, 243−252.
54. Hendsch, Z. S., and Tidor, B. (1999) Electrostatic interactions in the GCN4 leucine zipper: Substantial contributions arise from intramolecular interactions enhanced on binding, *Protein Sci. 8*, 1381−1392.
55. Sheinerman, F. B., and Honig, B. (2002) On the role of electrostatic interactions in the design of protein−protein interfaces, *J. Mol. Biol. 318*, 161−177.
56. Stone, A. J. (1996) in *The theory of intermolecular forces*, Oxford University Press, New York.
57. Jarque, C., and Buckingham, A. D. (1989) Ion−ion interaction in a polarizable lattice, *Chem. Phys. Lett. 164*, 485−490.
58. Tiede, D. M., Vashishta, A. C., and Gunner, M. R. (1993) Electron transfer kinetics and electrostatic properties of the *Rhodobacter sphaeroides* reaction center and soluble *c* cytochromes, *Biochemistry 32*, 4515−4531.
59. Adir, N., Axelrod, H. L., Beroza, P., Isaacson, R. A., Rongey, S. H., Okamura, M. Y., and Feher, G. (1996) Co-crystallization and characterization of the photosynthetic reaction center cytochrome c_2 complex from *Rhodobacter sphaeroides*, *Biochemistry 35*, 2535−2547.
60. Onuchic, J. N., Nymeyer, H., Garcia, A. E., Chahine, J., and Socci, N. D. (2000) The energy landscape theory of protein folding: Insights into folding mechanisms and scenarios, *Adv. Protein Chem. 53*, 87−152.
61. Israelachvili, J., and Wennerstrom, H. (1996) Role of hydration and water structure in biological and colloidal interactions, *Nature 379*, 219−225.
62. Zhou, H. X. (2001) Disparate ionic-strength dependencies of on and off rates in protein−protein association, *Biopolymers 59*, 427−433.
63. Selzer, T., and Schreiber, G. (1999) Predicting the rate enhancement of protein complex formation from the electrostatic energy of interaction, *J. Mol. Biol. 287*, 409−419.
64. Tezcan, F. A., Crane, B. R., Winkler, J. R., and Gray, H. B. (2001) Electron tunneling in protein crystals, *Proc. Natl. Acad. Sci. U.S.A. 98*, 5002−5006.
65. Hoffman, B. M., and Ratner, M. A. (1987) Gated electron transfer: When are observed rates controlled by conformational interconversion, *J. Am. Chem. Soc. 109*, 6237−6243.
66. Fersht, A. (1999) Structure and mechanism in protein science: A guide to enzyme catalysis and protein folding, W. H. Freeman, New York.
67. Onuchic, J. N., Luthey-Schulten, Z., and Wolynes, P. G. (1997) Theory of protein folding: The energy landscape perspective, *Annu. Rev. Phys. Chem. 48*, 545−600.

BI0350250